View Article Online / Journal Homepage / Table of Contents for this issue
Dynamic Article Links

PCCP

Cite this: *Phys. Chem. Chem. Phys.*, 2011, **13**, 8977–8984

www.rsc.org/pccp

PAPER

Charge controlled changes in the cluster and spin dynamics of $Sc_3N@C_{80}(CF_3)_2$: the flexible spin density distribution and its impact on ESR spectra†

Alexey A. Popov*[ab] and Lothar Dunsch[a]

Received 7th October 2010, Accepted 10th March 2011
DOI: 10.1039/c0cp02070b

Cluster and spin dynamics of a $Sc_3N@C_{80}(CF_3)_2$ derivative are studied by DFT in different charge states, from −3 to +1. For the neutral $Sc_3N@C_{80}(CF_3)_2$, static DFT computations of many cluster conformers as well as Born–Oppenheimer molecular dynamics (BOMD) show that addition of two CF_3 groups to $Sc_3N@C_{80}$ significantly changes dynamics of the Sc_3N cluster: instead of free rotation as in $Sc_3N@C_{80}$, the cluster in $Sc_3N@C_{80}(CF_3)_2$ exhibits only hindered motions. Similar cluster dynamics is found in the mono- and trianions of $Sc_3N@C_{80}(CF_3)_2$, while free rotation of the cluster is found in the cation. In the radical species, motions of the cluster dramatically change spin-density distribution. Spin populations of the metal atoms and the carbon cage are followed along the BOMD trajectories to reveal the details of the spin-flow. ^{45}Sc ESR hyperfine coupling constants integrated over BOMD trajectories are found to be substantially different from the results of static DFT computations, which emphasizes that cluster dynamics should be taken into account for reliable predictions of spectroscopic properties.

Published on 01 April 2011. Downloaded by Michigan State University on 22/01/2016 10:38:45.

1. Introduction

One of the most fascinating properties of endohedral metallofullerenes (EMFs) is their ability to stabilize the endohedral species which are not stable or not known to exist without the carbon cage.[1–7] The most apparent example is the family of nitride clusterfullerenes, $M_3N@C_{2n}$ (M = Sc, Y, lanthanides; $2n$ = 68–96), in which trimetallic nitride clusters (which have never been observed outside the carbon cage) are encapsulated inside the carbon cages of different size and symmetry.[8] A prominent member of this family, $Sc_3N@C_{80}$-$I_h(7)$, is the third most abundant fullerene after C_{60} and C_{70}.[9] Even though the endohedral clusters in EMFs are shielded from the environment by the carbon cage, the electronic structure of the endohedral species can be tuned by the exohedral chemical modification of the fullerene cage.[10–13] Charging the EMF molecule can also affect the electronic state of the endohedral cluster, and this effect can be especially strong if frontier orbitals of the EMF molecule have large contributions from the metal atoms.[14–19]

$Sc_3N@C_{80}$ is known to have its LUMO localized on the endohedral cluster, which results in a large hyperfine coupling constant (hfcc) observed in the ESR spectra of its anion: $a(^{45}Sc)$ = 55–57 Gauss.[17,20] Exohedral modification of the carbon cage can significantly alter frontier orbitals, and in our recent ESR spectroelectrochemical study of the charged states of 1,4-adduct $Sc_3N@C_{80}(CF_3)_2$ we have shown that both LUMO and LUMO + 1 orbitals of the perfluoroalkyl derivative have significant cluster contributions leading to noticeable hfcc values in the ESR spectra of the mono- and trianions.[21] Importantly, modelling of the experimental ESR spectra required two different $a(^{45}Sc)$ values, 9.34 (×2) and 10.70 Gauss in the monoanion, and 10.8 (×2) and 49.2 Gauss in the trianion, which points to a hindered rotation of the Sc_3N cluster in the derivative.[21] Hindered rotation of the endohedral cluster was also revealed by ESR spectroscopy for $Sc_3N@C_{80}(CF_3)_{10}$ and $Sc_3N@C_{80}(CF_3)_{12}$ anions[22] as well as for the pyrrolidine adduct of $Sc_3C_2@C_{80}$.[23]

Theoretical studies of the spin-density distribution in anion-radicals can strongly help in understanding the spin states of such species and interpret experimental ESR spectra. However, in addition to the standard difficulties known in predictions of hfcc values for transition metals (see ref. 24 and 25), an additional problem in the studies of EMFs is caused by the dynamics of the endohedral cluster. For instance, Sc_3N is known to rotate freely inside $Sc_3N@C_{80}$,[9,16,26] and to a large extent this is also true for its monoanion.[27] As a result,

[a] *Department of Electrochemistry and Conducting Polymers, Leibniz-Institute for Solid State and Materials Research (IFW Dresden), D-01171 Dresden, Germany. E-mail: a.popov@ifw-dresden.de; Fax: +49 351 4659 811; Tel: +49 351 4659 658*
[b] *Chemistry Department, Moscow State University, Moscow 119992, Russia*

† Electronic supplementary information (ESI) available: Cartesian coordinates and relative energies of conformers of $Sc_3N@C_{80}(CF_3)_2$ in different charge states, instant hfcc values along BOMD trajectories, spin populations in a $Sc_3N@C_{80}(CF_3)_2^+$ cation-radical as a function of time, spin population of Sc atoms in a $Sc_3N@C_{80}(CF_3)_2^-$ anion radical along the reaction coordinate. See DOI: 10.1039/c0cp02070b

View Article Online

Published on 01 April 2011. Downloaded by Michigan State University on 22/01/2016 10:38:45.

experimentally measurable properties correspond to the time-averaged situation (the time scale can reach a nanosecond diapason as in ESR and NMR spectroscopies). Thus, when predicting the spectroscopic properties, this kind of internal dynamics should be taken into account.

Molecular dynamics (MD) simulations appear to be an ideal tool for addressing the problems of the cluster dynamics and its influence on spectroscopic properties, however the wide use of such methods is still hindered by the high computational costs, especially when long propagation times are necessary. For this reason, first principle MD studies of endohedral fullerenes are still very rare.[6,7,27–30] An important contribution to this field was made by the use of the density-functional based tight binding method (DFTB) to follow dynamics of the cluster in $Sc_3N@C_{80}$ over a nanosecond range to predict ^{13}C NMR spectra.[26] Computing NMR chemical shifts of carbon atoms after certain time intervals, the authors have shown that the cluster rotation indeed results in the averaging of the chemical shifts in agreement with experimental finding. Importantly, the properties predicted *via* a dynamic approach are in better agreement with experimental data than the results of static computations even for C_{60}.[26]

In this work we address the question of the influence of charge on the cluster and spin dynamics in $Sc_3N@C_{80}(CF_3)_2$ using DFT and Born–Oppenheimer molecular dynamics (MD). We show that spin density in $Sc_3N@C_{80}$ and its derivatives is very flexible and exhibits strong variation in a short timescale (the effect known as spin-flow). Thus, it is important to take the cluster dynamics into account when analyzing the ESR spectra of charged structures and predicting hfcc values. We show that even relatively short propagation times of several picoseconds can be already sufficient to give the realistic description of the cluster dynamics.

2. Results and discussion

2.1 Cluster-cage conformers of $Sc_3N@C_{80}(CF_3)_2$

It is well established both experimentally and theoretically that the Sc_3N cluster is freely rotating inside an icosahedral C_{80} cage, both at NMR- and ESR-relevant time scales. DFT studies show that there are several conformers of $Sc_3N@C_{80}$ with very similar relative energies and with the barriers to rotation (the energies of transition states) within the range of 10 kJ mol^{-1}.[16,31,32] In combination with the high symmetry of the carbon cage, it results in multiple equivalent energy minima, and the cluster "rotation" trajectory can be described as a jumping between these minima. Exohedral modification of the carbon cage can significantly change dynamics of the endohedral cluster by introducing more preferable sites for the cluster bonding. For instance, our preliminary calculations of $Sc_3N@C_{80}(CF_3)_2$ in its neutral state have shown that the energies of conformers span the range of at least 60 kJ mol^{-1}[11] (*vs.* the aforementioned value of 10 kJ mol^{-1} in $Sc_3N@C_{80}$). Furthermore, charging the molecule can also significantly affect the cluster dynamics.[16]

To get a deeper insight into the influence of these two factors for $Sc_3N@C_{80}(CF_3)_2$, we have performed detailed studies of possible conformers of +1, 0, −1, and −3 charge states by optimizing the structures with up to 50 different initial orientations of the cluster (see ESI† for more details). This procedure resulted in 30–40 different conformers for each charge state. In agreement with our preliminary findings,[11] for the neutral $Sc_3N@C_{80}(CF_3)_2$ we have found two especially stable conformers (**Cnf1** and **Cnf2**, ΔE = 0.0 and 1.7 kJ mol^{-1}, respectively). Both structures have C_1 symmetry with one Sc atom (Sc3) facing the hexagon on the opposite side of the $C_6(CF_3)_2$ fragment. The differences between two conformers are in the relative position of this atom with respect to the pentagon/hexagon (pent/hex) edge (Fig. 1). A C_2-symmetric conformer with the Sc3 atom facing exactly the centre of the hexagon is a transition state (**TS1**, ΔE = 2.9 kJ mol^{-1}) between two equivalent conformers (**Cnf1** and **Cnf1′**), while the energy of the transition state between **Cnf1** and **Cnf2** structures (**TS2**) is 3.9 kJ mol^{-1}. Importantly, conformations of the Sc_3N cluster in **Cnf1** and **Cnf2** correspond well to the conformations of the cluster in two other 1,4-derivatives of $Sc_3N@C_{80}$ described in the literature, bis-silylated $Sc_3N@C_{80}((Mes_2Si)_2CH_2)$[33] and dibenzyl derivative $Sc_3N@C_{80}(CH_2C_6H_5)_2$,[34] whose structures were determined by single-crystal X-ray diffraction studies. Nagase and Kobayashi have found that due to the large degree of ionic bonding, positions of the metal atoms in EMFs correspond to the minima of the electrostatic potential of the appropriately charged empty cage.[35] Fig. 2 shows electrostatic potential isosurfaces in $C_{80}(CF_3)_2^{6-}$ (the Sc_3N cluster formally donates 6 electrons to the carbon cage). It can be seen that the position of the Sc atom opposite to the $C_6(CF_3)_2$ hexagon is indeed supported by the spatial distribution of electrostatic potential in the empty hexaanion.

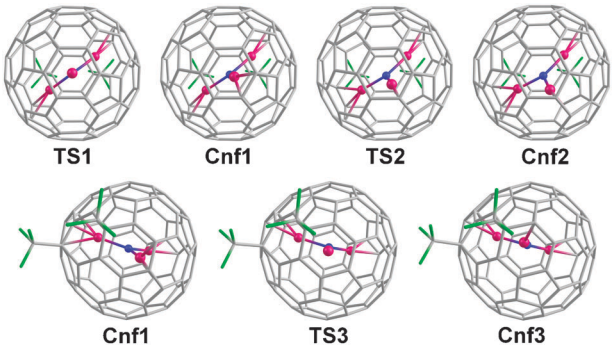

Fig. 1 PBE/TZ2P-optimized structures of the lowest energy conformers of $Sc_3N@C_{80}(CF_3)_2$ and its anions. In the top row molecules are oriented along the 2-fold axis of a $C_{80}(CF_3)_2$ moiety to emphasize the changes of the position of Sc3 in the **TS1** → **Cnf1** → **TS2** → **Cnf2** sequence. In the bottom row orientation of the molecules emphasizes changes of the position of Sc1 in the **Cnf1** → **TS3** → **Cnf3** sequence.

In all structures discussed so far (**Cnf1**, **Cnf2**, **TS1**, and **TS2**) two other Sc atoms occupy almost identical positions, being close to carbon atoms in *para* positions with respect to the C-sp^3 atoms. It is now well established for the empty fullerenes that CF_3 groups tend to form ribbons of edge-sharing *p*- or *m*-$C_6(CF_3)_2$ hexagons.[36–41] To some extent, this tendency can be also found for $Sc_3N@C_{80}$, if the term "ribbon" is generalized to the Sc-bonded carbon atoms. That is, in two lowest energy conformers of $Sc_3N@C_{80}(CF_3)_2$, the C(Sc)–C(CF_3)–C(CF_3)–C(Sc) sequence

 This journal is © the Owner Societies 2011

View Article Online

Published on 01 April 2011. Downloaded by Michigan State University on 22/01/2016 10:38:45.

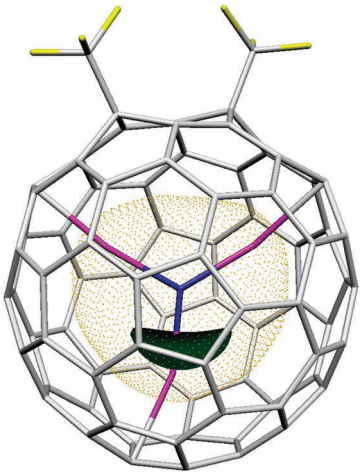

Fig. 2 Electrostatic potential (ESP) in $C_{80}(CF_3)_2^{6-}$ computed at the B3LYP/6-311G* level superimposed with the position of the Sc_3N cluster in **Cnf1**. Two isosurfaces are shown: −0.605 a.u. (solid, green) and −0.600 a.u. (dots, orange).

forms the *para–para–para–para* ribbon. When Sc1 or Sc2 atoms are moved toward different positions (breaking thus the ribbon), the energy rises to at least 13.0 kJ mol^{-1}, and even higher energy conformers are obtained if the cluster is reoriented further. In total, from 33 conformers found for the non-charged $Sc_3N@C_{80}(CF_3)_2$, only two aforementioned conformers are found in the range of 0–10 kJ mol^{-1}, three conformers are in the range of 10–20 kJ mol^{-1}, while other 28 span the range of 20–65 kJ mol^{-1}. Thus, based on these results it can be expected that rotation of the Sc_3N cluster is significantly hindered in $Sc_3N@C_{80}(CF_3)_2$ as compared to that in $Sc_3N@C_{80}$.

Enhanced stability of **Cnf1** and **Cnf2** is preserved in the monoanion and trianion. **Cnf1** is the most stable conformer in both charge states, while **Cnf2** is 5.5 and 7.8 kJ mol^{-1} less stable in the mono- and trianionic states, respectively. In the monoanion, the two conformers are separated by a gap of 16.5 kJ mol^{-1} from the third most stable conformer (ΔE = 23.0 kJ mol^{-1}), and 37 other conformers of the monoanion span the range of 23–64 kJ mol^{-1}. For the trianion we have found one additional stable isomer (**Cnf3**, ΔE = 6.6 kJ mol^{-1}), in which the Sc1 atom is facing the center of the hexagon bearing one CF_3 group (Fig. 1). The fourth stable isomer has a relative energy of 18.8 kJ mol^{-1}, and 30 other conformers span the energy range of 28–69 kJ mol^{-1}.

In contrast to the non-charged $Sc_3N@C_{80}(CF_3)_2$ and its anions, there are no specifically preferred cluster conformers for the cation. The distribution of the conformers is very dense: there are 11 structures within the range of 10 kJ mol^{-1}, 15 more structures span the range of 10–20 kJ mol^{-1}, and 12 conformers are found in the range of 20–49 kJ mol^{-1}. This distribution is drastically different from that in the neutral state and in the anions, in which only few stable structures are found within the range of 0–20 kJ mol^{-1} with the majority of conformers having their relative energies above 20 kJ mol^{-1}. The energy range spanned by the conformers and their distribution in this range allows the preliminary conclusion on the dynamical behaviour of the cluster. Enhanced stability of two to three conformers points to the restricted motion, while dense distribution of the conformers can be an indication of the (almost) free rotation. It is thus apparent that conformational behavior of the cluster is substantially different in the cationic state of the fullerene and that the cluster may rotate much easier than in the other charge states considered in this work.

Description of the cluster dynamics based on the relative energies of conformers cannot be complete since the barriers to rotation remain unknown, and one cannot exclude high barriers to rotation (and thus hindered rotation) even for the densely distributed conformers. Global search of transition states connecting the conformers such as that reported by us for $Sc_3N@C_{80}$[16] and $TiSc_2N@C_{80}$[27] might answer the question, but for $Sc_3N@C_{80}(CF_3)_2$ this approach appears to be impractical for a large number of the conformers. Instead, to address the question of the cluster rotation, we have performed Born–Oppenheimer molecular dynamics (BOMD) simulation to follow the dynamics of the cluster in the picosecond time scale. Fig. 3 shows trajectories of the endohedral cluster in the different charge states of $Sc_3N@C_{80}(CF_3)_2$ obtained in the microcanonical ensemble after equilibration at 300 K. It can be clearly seen that the cluster in the mono- and trianions of $Sc_3N@C_{80}(CF_3)_2$ exhibits a similar type of motions, which to a large extent can be described as restricted motion between two lowest energy conformers. Similar cluster dynamics was also found for the non-charged $Sc_3N@C_{80}(CF_3)_2$ (not shown). In line with the distribution of the conformer energies, BOMD shows that the cluster in the cation rotates almost freely. For comparison, analogous BOMD simulations for $Sc_3N@C_{80}$ and its monoanion have shown that the cluster exhibits free rotation at the time scale of several picoseconds[27] (that is, the trajectories look similar to that shown in Fig. 3c for the cation).

2.2 Spin-flow in $Sc_3N@C_{80}(CF_3)_2^-$ and $Sc_3N@C_{80}(CF_3)_2^{3-}$

In our recent study of the conformers of $Sc_3N@C_{80}^-$ we have found that even a slight reorientation of the cluster results in large changes of the Sc spin populations and hyperfine splitting constant.[16] Thus, dynamics of the cluster can substantially affect the spin-density distribution, and hence this effect should be taken into account when predicting hfcc values for such molecules. In this respect, we have followed Mulliken spin populations of the Sc atoms in $Sc_3N@C_{80}(CF_3)_2^-$ and $Sc_3N@C_{80}(CF_3)_2^{3-}$ over the BOMD trajectories. Recently, a

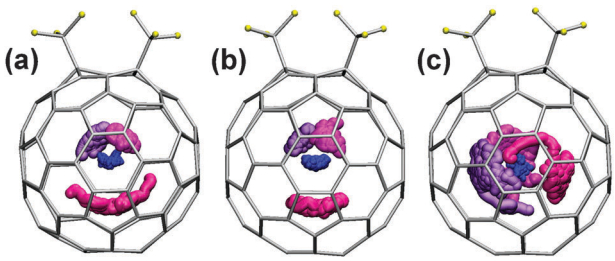

Fig. 3 BOMD (12 ps, 300 K, PBE/DZ(P)) trajectories of $Sc_3N@C_{80}(CF_3)_2^-$ (a), $Sc_3N@C_{80}(CF_3)_2^{3-}$ (b), and $Sc_3N@C_{80}(CF_3)_2^+$ (c). Nitrogen—blue, Sc—different shades of violet, displacement of carbon and fluorine atoms is not shown.

View Article Online

Published on 01 April 2011. Downloaded by Michigan State University on 22/01/2016 10:38:45.

similar analysis was reported by us for $Sc_3N@C_{80}^-$ and $TiSc_2N@C_{80}$.[27]

For optimized structures of conformers **Cnf1** and **Cnf2**, the largest spin populations at the PBE/DZ(P) level are predicted for Sc1 or Sc2 (0.36 and 0.09, respectively, in **Cnf1**; 0.18 and 0.25, respectively, in **Cnf2**); note that dynamics of the cluster implies that the values averaged over time should be identical for these two atoms. For Sc3, the spin populations are 0.28 for **Cnf1** and 0.11 for **Cnf2**. Hybrid functionals (in particular, PBE0 was tested in this work, see below) give qualitatively the same predictions, but the spin populations of the metal atoms are somewhat lower, while that of the carbon cage is somewhat higher than the values predicted with the use of GGA functionals.[27] Analysis of the variation of the spin population over BOMD trajectories shows that static computations "hide" important details of the spin density distribution. Fig. 4a shows that spin populations of all Sc atoms in $Sc_3N@C_{80}(CF_3)_2^-$ oscillate very rapidly in the range from almost 0 to 0.6. More detailed analysis shows that the spin population trajectory of Sc2 is the mirror image of the spin population trajectory of Sc1. That is, the sum of spin populations of Sc1 and Sc2 atoms always remains close to 0.4 and exhibits much smaller variations in time than spin populations of individual atoms (Fig. 4a). On the other hand, it can be seen as well that the curves representing time dependencies of the net spin population of the whole cluster and spin population of the Sc3 atom are almost identical

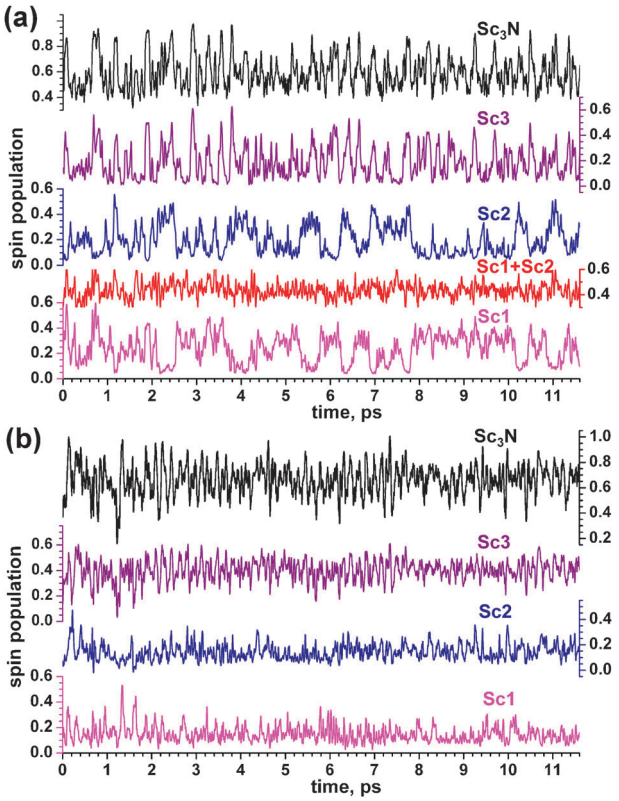

Fig. 4 Spin populations of Sc atoms and net spin population of the Sc_3N cluster in $Sc_3N@C_{80}(CF_3)_2^-$ (a) and $Sc_3N@C_{80}(CF_3)_2^{3-}$ (b) as a function of time obtained in BOMD simulations (300 K, PBE/DZ(P) level).

except for the shift in the ordinate scale (the time-averaged spin population of Sc3 is 0.19, while that of the whole cluster is 0.60). It is thus obvious that the spin density distribution in $Sc_3N@C_{80}(CF_3)_2^-$ is very flexible, and that the spin-flow dynamics can be partitioned into two almost independent processes: (i) the intracluster spin-flow between Sc1 and Sc2, and (ii) the spin flow between Sc3 and the carbon cage. Importantly, while static computations for **Cnf1** and **Cnf2** predict larger spin populations for Sc1/Sc2 atoms as compared to Sc3, the values averaged over BOMD trajectory are very similar for all three atoms. Obviously, predictions of the hyperfine splitting constants of Sc atoms that do not take dynamical flexibility of the spin density distribution and rely only on static computations can be even qualitatively incorrect.

Time dependencies of spin populations of Sc atoms in $Sc_3N@C_{80}(CF_3)_2^{3-}$ are shown in Fig. 4b. For Sc1 and Sc2 time-averaged spin populations are 0.14, and the range of their variations with the cluster motions, ± 0.15, is considerably smaller than that in the monoanion. Spin populations of Sc3 oscillate around 0.40 in the range of *ca.* ± 0.15 with few dips and spikes down to 0 or up to 0.6. The variations of the net spin population of the Sc_3N cluster resemble those of Sc3, however the magnitude of variations is *ca.* 1.5 times higher for the whole cluster than for the individual Sc atoms; the time-averaged net spin population is 0.66. Thus, spin density dynamics in the trianion has a more complex mechanism than in the monoanion and involves intracluster and metal-cage spin-flow for all three Sc atoms.

For $Sc_3N@C_{80}^-$, variations of the spin populations for individual Sc atoms are also in the range of 0.29 ± 0.25, while the net spin population of the Sc_3N cluster oscillates in the range 0.83 ± 0.15. Therefore, the total situation can be also described as spin-flow both between Sc atoms within the cluster as well as between the cluster and the cage.[27]

In contrast to anions, we did not find for the cation significant changes of the spin population of Sc atoms over the trajectory (see Fig. S1 in ESI†). Time-averaged values for individual Sc atoms do not exceed 0.05, and the maximum instant values are less than 0.10.

2.3 ^{45}Sc ESR hyperfine coupling constants

Hfccs and BOMD simulations. In the view of the flexibility of the spin density distribution, we have analyzed the influence of the dynamics of the cluster on the $a(^{45}Sc)$ hyperfine coupling constants (hfccs). High-quality predictions of hfccs require the use of hybrid functionals and large basis sets with an extended core region.[16,25] The use of such approaches in BOMD of large molecules is still not feasible, and the results discussed below are based on GGA PBE calculations with {6,5,3,1}/(19s,15p,11d,5f) basis sets for Sc atoms and the DZ-quality {3,2}/(7s,4p) basis set for the carbon cage. Although this approach can hardly give quantitative agreement with experimental data, the general trends are expected to be predicted correctly.

Fig. 5 shows trajectory-averaged hfccs for each Sc atom in $Sc_3N@C_{80}^-$ as a function of the propagation time (instant hfccs as a function of time are shown in ESI†).

 This journal is © the Owner Societies 2011

View Article Online

Published on 01 April 2011. Downloaded by Michigan State University on 22/01/2016 10:38:45.

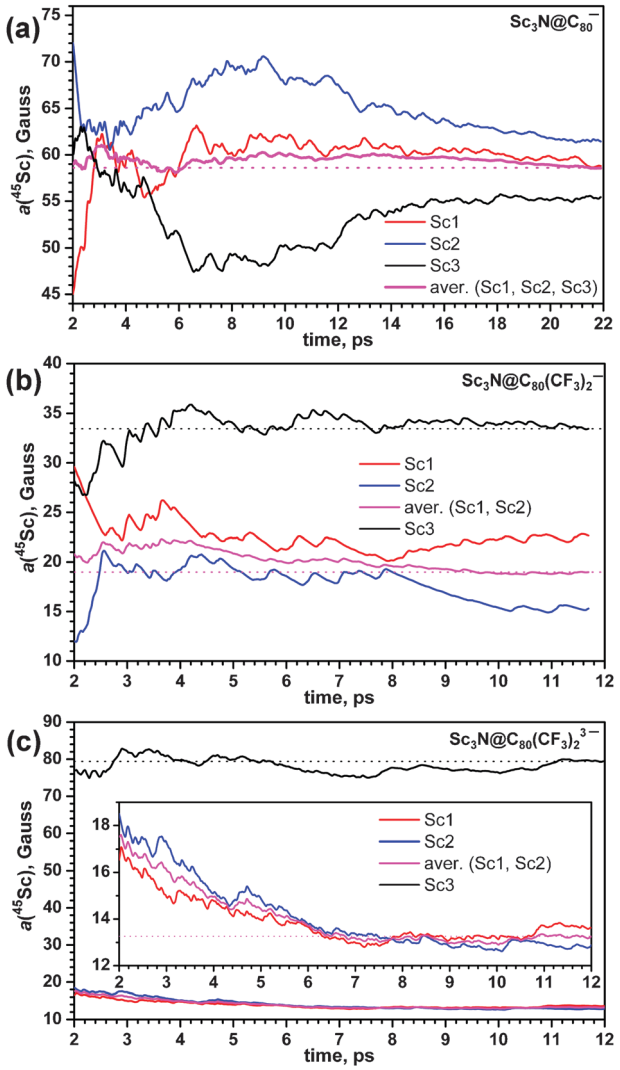

Fig. 5 Time-averaged $a(^{45}Sc)$ values in $Sc_3N@C_{80}^-$ (a), $Sc_3N@C_{80}(CF_3)_2^-$ (b) and $Sc_3N@C_{80}(CF_3)_2^{3-}$ (c) as a function of propagation time (BOMD simulations, 300 K, PBE/DZ(P) level). Large oscillations of $a(^{45}Sc)$ values during the first two picoseconds are not shown.

Due to the isotropic rotation of the cluster, all three hfccs should converge to the same value in the infinite time limit. It can be seen in Fig. 5a that propagation for 20 ps is still not sufficient to achieve such a convergence (note that the ESR-relevant time scale is in the order of nanoseconds). However, the values are already rather similar, the largest deviations from the mean value not exceeding 5 Gauss. Importantly, the mean $a(^{45}Sc)$ value (averaged over three Sc atoms) converges much faster than the values for individual atoms, and variation of the mean hfcc does not exceed 1–2 Gauss already beyond 6 ps (converged value at 22 ps is 59 Gauss). The limit of 59 Gauss was also obtained in two other BOMD runs for $Sc_3N@C_{80}^-$ with different initial conditions (see ESI†), thus confirming the reliability of this value.

In our earlier study of $Sc_3N@C_{80}^-$ we have found that the lowest energy conformer had C_{3v} symmetry, and that $a(^{45}Sc)$ values predicted for this conformer even with the use of hybrid functionals with extended basis sets underestimated the experimental hfcc (*ca.* 56 Gauss) by at least 30%.[16] Static computations for the C_{3v} conformer at the PBE/DZ(P) level give $a(^{45}Sc) = 47$ Gauss, which is also about 20% smaller than the value obtained at the same level of theory in BOMD calculations. It should be noted that although 59 Gauss obtained in BOMD is very close to the experimental value of 56 Gauss, this is probably a result of fortuitous cancellation of errors rather than exact prediction, since the PBE/DZ(P) level is not sufficient for adequate predictions of hfcc values. Yet, the fact that dynamics of the cluster significantly increases DFT-predicted $a(^{45}Sc)$ is a very important finding showing that this factor has to be taken into account to make reliable predictions of hfcc values in endohedral metallofullerenes with flexible positions of the endohedral species.

Hfccs obtained by the integration over BOMD trajectories of $Sc_3N@C_{80}(CF_3)_2^-$ and $Sc_3N@C_{80}(CF_3)_2^{3-}$ are shown in Fig. 5b and c. The integration period of 12 ps is again not sufficient to get fully converged values, but the general trends can be clearly seen at this time scale. Most importantly, for $Sc_3N@C_{80}(CF_3)_2^-$ BOMD predicts a considerably higher $a(^{45}Sc)$ value for Sc3 than for Sc1 and Sc2 (the mean value for two latter atoms also converges much faster than individual values). Taking into account higher spin populations of Sc1 and Sc2 either in static (for **Cnf1** and **Cnf2**) or BOMD calculations (see the previous section) this result is counter-intuitive, but it agrees reasonably with the experimental spectrum, which also shows a higher $a(^{45}Sc)$ value for Sc3 (10.7 Gauss) in comparison to Sc1 and Sc2 (9.3 Gauss).[21] Results of BOMD calculations for $Sc_3N@C_{80}(CF_3)_2^{3-}$ are closer to those expected by BOMD spin populations analysis as well as by the spin density distribution in the energy minima. All calculations show enhanced spin population and much higher hfcc for Sc3 than for Sc1 and Sc2, which agrees well with the experimental data ($a(^{45}Sc)$ is 49.2 Gauss for Sc3 and 10.8 Gauss for Sc1 and Sc2, see ref. 21).

Hfccs and intrinsic reaction coordinate calculations. Large variations of the instant spin populations and hfccs within the internal motions of the cluster stimulate a more detailed study of this phenomenon. Hence, we have performed additional computations of hfccs along the specially chosen trajectory of the cluster. With respect to the results of BOMD simulations on the cluster dynamics, the best choice of the trajectory to follow hfccs is the reaction coordinate connecting **Cnf1** and **Cnf2** conformers (in $Sc_3N@C_{80}(CF_3)_2^{3-}$, a path to **Cnf3** is also included). To do so, we have first found transition states between these conformers and performed intrinsic reaction coordinate (IRC) calculations to obtain the trajectories. Energy profiles along the reaction coordinate obtained at the PBE/TZ2P level are shown in Fig. 6 and 7. Note that C_2-symmetry of the $C_{80}(CF_3)_2$ moiety implies that the reaction coordinate can be followed only from **Cnf2** to **Cnf1** and till the transition state (**TS1**) connecting **Cnf1** and its symmetry equivalent conformer denoted hereafter as **Cnf1′**. The "total" symmetry of $Sc_3N@C_{80}(CF_3)_2$ is however lower than the symmetry of $C_{80}(CF_3)_2$, and hence Sc1 and Sc2 are not equivalent (except for **TS1**, in which $Sc_3N@C_{80}(CF_3)_2$ has rigorous C_2 symmetry). As a result (although energy profiles

View Article Online

Published on 01 April 2011. Downloaded by Michigan State University on 22/01/2016 10:38:45.

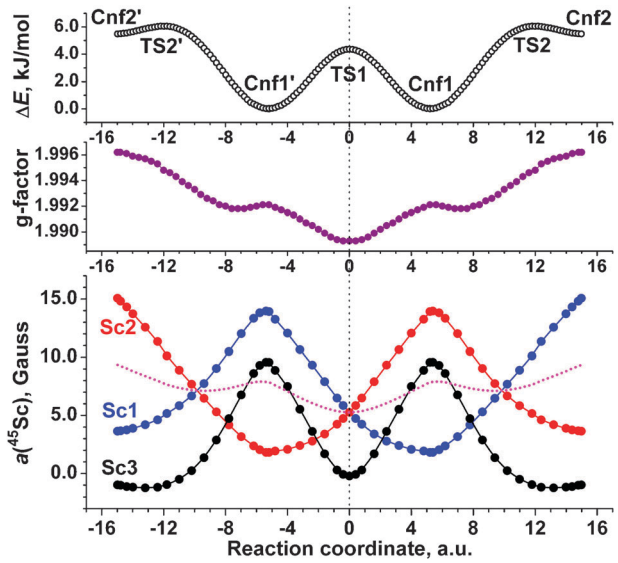

Fig. 6 DFT-computed relative energy (ΔE, PBE/TZ2P), g-factor (PBE/TZVP) and $a(^{45}Sc)$ constants (PBE0/(6-311G*, CP3P)) in $Sc_3N@C_{80}(CF_3)_2^-$ along the **Cnf2′** → **TS2′** → **Cnf1′** → **TS1** → **Cnf1** → **TS2** → **Cnf2** reaction coordinate. Dotted magenta line shows mean $a(^{45}Sc)$ value for Sc1 and Sc2.

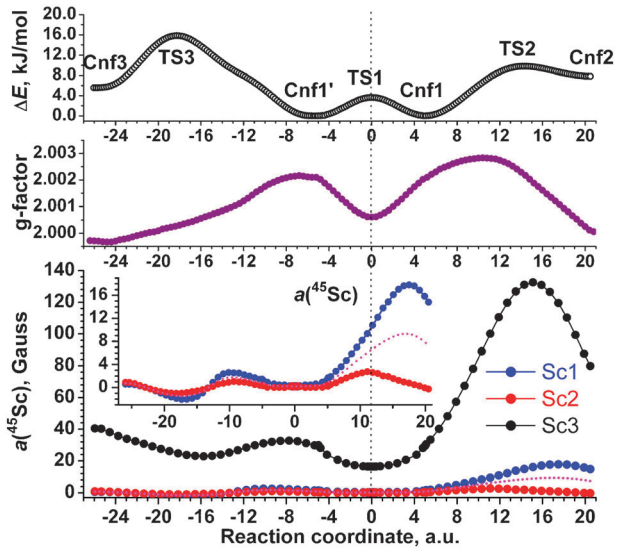

Fig. 7 DFT-computed relative energy (ΔE, PBE/TZ2P), g-factor (PBE/TZVP) and $a(^{45}Sc)$ constants (PBE0/(6-311G*, CP3P)) in $Sc_3N@C_{80}(CF_3)_2^{3-}$ along the **Cnf3** → **TS2** → **Cnf1′** → **TS1** → **Cnf1** → **TS2** → **Cnf2** reaction coordinate. Dotted magenta line shows the mean $a(^{45}Sc)$ value for Sc1 and Sc2.

along the **TS1** → **Cnf1** and **TS1** → **Cnf1′** pathways are identical), the properties of the Sc1 and Sc2 atoms are different in these two routes (in fact, Sc1 is equivalent to Sc2′ while Sc2 is equivalent to Sc1′). To illustrate this situation, we have plotted the energy profile of $Sc_3N@C_{80}(CF_3)_2^-$ along the **Cnf2** → **TS2** → **Cnf1** → **TS1** → **Cnf1′** → **TS2′** → **Cnf2′** trajectory (Fig. 6) (that is, in both symmetry-related directions with respect to **TS1**). For a number of points along this reaction coordinate, we have then computed hfccs using hybrid PBE0 functional and the special CP3P basis set for Sc atoms designed by Neese[42] for calculations of core properties (the standard 6-311G* basis set was employed for carbon, nitrogen and fluorine atoms). Besides, g-factor was computed for certain points along the reaction coordinate at the PBE/TZVP level using an effective potential/mean-field approach in "complete mean field" approximation.[43,44] Computed hfcc and g-factor values along the reaction coordinate are plotted in Fig. 6 as well.

In line with our earlier results on $Sc_3N@C_{80}^-$ and results of BOMD calculations described above, hfcc calculations along the reaction coordinate show that even slight motion of Sc atoms results in significant changes of hfcc values. Along the whole path from **Cnf2** to **Cnf2′** only Sc3 exhibits noticeable motions while displacements of Sc1 and Sc2 are hardly seen by eyes. However, even for such infinitesimal displacements, hfccs of Sc1 (Sc2) vary from 4 to 14 Gauss. The curves for Sc1 and Sc2 again look like mirror images: hfcc value is maximal for Sc1 when it is minimal for Sc2 (for instance, in **Cnf1**/**Cnf1′** or in **Cnf2**/**Cnf2′** pairs). As a result, the mean value exhibits much smaller variations than individual hfccs (*cf.* changes of the spin populations for Sc1 and Sc2 in Fig. 4). Hfcc of Sc3 also changes significantly, from −1 to 10 Gauss. Importantly, the maximum value for Sc3 is found for **Cnf1**/**Cnf1′**, the lowest energy conformers, and only in the vicinity of these conformers the $a(^{45}Sc3)$ value is larger than the mean Sc1/Sc2 hfcc. It should be noted that the range of hfccs obtained at the PBE0 level is much closer to the experimental values (~10 Gauss) than the results of GGA calculations.

Fig. 7 shows analogous data for $Sc_3N@C_{80}(CF_3)_2^{3-}$, however the **Cnf1′** → **TS2′** → **Cnf2′** path is not shown; instead, Fig. 7 plots computed relative energy and ESR parameters along the **Cnf1′** → **TS3′** → **Cnf3′** pathway. Large variations of hfcc values with displacement of Sc atoms are obvious. This is especially well seen for Sc3, in which $a(^{45}Sc)$ value reaches up to 130 Gauss between **TS2** and **Cnf2**. At the same time, on the **TS1** → **Cnf1** → **TS3** → **Cnf3** pathway the values do not exceed 40 Gauss. Much smaller hfccs are predicted for Sc1 and Sc2: on the **TS1** → **Cnf1** → **TS3** → **Cnf3** pathway, the values do not exceed 4 Gauss, and only along the **TS2** → **Cnf2** part of the trajectory $a(^{45}Sc)$ values for Sc1 and Sc2 reach 18 Gauss.

Computations of g-factors along the reaction coordinate show that this parameter is also noticeably sensitive to the displacements of the cluster. The range of values predicted for $Sc_3N@C_{80}(CF_3)_2^-$ (1.9893–1.9962) and $Sc_3N@C_{80}(CF_3)_2^{3-}$ (1.9997–2.0028) agrees well with experimental data (1.9958 and 2.0006 for mono- and trianions, respectively).[21]

3. Computational details

Optimization of the molecular structures of all species reported in this work was performed using PBE functional[45] and the TZ2P-quality basis set (full-electron {6,3,2}/(11s,6p,2d) for C, N, and F atoms, and SBK-type effective core potential for Sc atoms with {5,5,4}/(9s,9p,8d) valence part) implemented in the PRIRODA package.[46,47] This basis set is abbreviated in the manuscript as "TZ2P". The code employed expansion of the electron density in an auxiliary

 This journal is © the Owner Societies 2011

View Article Online

Published on 01 April 2011. Downloaded by Michigan State University on 22/01/2016 10:38:45.

basis set to accelerate evaluation of the Coulomb and exchange–correlation terms.[46] All charged radical states were studied in their doublet state. For IRC computations, transition states (**TS**s) connecting energy minima were found first and their nature was confirmed by the presence of one imaginary frequency in Hessian computations. Then, the system was allowed to relax by following the normal coordinates corresponding to imaginary frequencies.

The Velocity Verlet algorithm with the time step of 1.5 fs was used in Born–Oppenheimer molecular dynamics (BOMD) calculations. The energies and gradients were computed with the PRIRODA package using PBE functional, double-zeta quality {3,2}/(7s,4p) basis-set for cage carbon atoms and DZP-quality basis sets for N, Sc and CF_3 groups (Sc: {6,5,3,1}/(19s,15p,11d,5f); N, C, F: {3,2,1}/(10s,7p,3d)). Molecules were first equilibrated at 300 K for 0.6 ps by rescaling velocities when the deviation of the instant temperature from 300 K exceeded 20 K. Then, the trajectory was followed without a thermostat (*i.e.*, in microcanonical ensemble).

Additional computations of hfcc values were performed with the Firefly package[48] using hybrid PBE0 (also known as PBE1PBE) functional, 6-311G* basis set for C, N, and F atoms, and CP3P basis set ({17,7,3,1}/(17s,11p,5d,1f)) for Sc atoms. Calculations of g-factors were performed with the ORCA package[49] at the PBE/TZVP[50] level using the mean-field method implemented in ORCA.

4. Conclusions

In this work we have performed a thorough study of the internal cluster and spin dynamics in $Sc_3N@C_{80}(CF_3)_2$ in different charge states and the influence of this dynamics on the spectroscopic properties, in particular, on ^{45}Sc hyperfine coupling constants. This study has shown that exohedral modification by addition of two CF_3 groups to a C_{80} cage drastically affects the dynamics of the endohedral Sc_3N cluster. Instead of free rotation, which the cluster exhibits in $Sc_3N@C_{80}$, in the derivative and its anions the cluster motions are restricted. At the same time, in the $Sc_3N@C_{80}(CF_3)_2^+$ cation rotation of the cluster reappears.

Dynamics of the cluster has a dramatic impact on the spin density distribution in the radical anions. Molecular dynamics simulations show that even slight shifts of the Sc atoms from their positions result in strong changes of their spin populations, which altogether can be described as a spin-flow both between the Sc atoms and between the cluster and the fullerene cage. The dynamic nature of the spin density distribution has to be taken into account in determinations of the ESR hfcc values by DFT. We have found that the failures of the previous DFT results for the ^{45}Sc hfcc constant in a $Sc_3N@C_{80}^-$ anion can be explained by the static nature of those calculations: the hfcc values averaged over BOMD trajectories are noticeably larger than the values computed for the lowest energy conformers. Importantly, while fully converged hfcc values in BOMD simulation would require long propagation times and are still hardly feasible at the DFT level, our simulations also show that the mean values for dynamically-equivalent atoms require only several picoseconds to converge. Thus, reasonable results can be obtained for much shorter time and hence such a procedure is strongly recommended for prediction of hfcc values of molecules with flexible spin density distribution. The best results should be obtained when BOMD simulations for the cluster dynamics are coupled with hybrid DFT calculations with extended basis sets for computations of hfcc values for the atoms of interest. In this way the change in cluster dynamics by charging the endohedral fullerene and the influence of these phenomena on the ESR spectra can be described with high accuracy.

Acknowledgements

This work was supported by Alexander von Humboldt Foundation (fellowship to A. A. P.). A. A. P. acknowledges "Chebyshev SKIF-MSU" supercomputer team in Moscow State University for a computer time. Technical assistance of U. Nitzsche with local computer resources in IFW is highly appreciated. The authors are thankful to N. Shustova, S. Strauss, O. Boltalina, and S. Stevenson for a fruitful collaboration in the studies of the derivatives of $Sc_3N@C_{80}$.

Notes and references

1 H. Shinohara, *Rep. Prog. Phys.*, 2000, **63**, 843–892.
2 *Endofullerenes: A New Family of Carbon Clusters*, ed. T. Akasaka and H. Nagase, Kluwer, Dordrecht, 2002.
3 M. N. Chaur, F. Melin, A. L. Ortiz and L. Echegoyen, *Angew. Chem., Int. Ed.*, 2009, **48**, 7514–7538.
4 L. Dunsch and S. F. Yang, *Phys. Chem. Chem. Phys.*, 2007, **9**, 3067–3081.
5 A. A. Popov, *J. Comput. Theor. Nanosci.*, 2009, **6**, 292–317.
6 L. Dunsch, S. Yang, L. Zhang, A. Svitova, S. Oswald and A. A. Popov, *J. Am. Chem. Soc.*, 2010, **132**, 5413–5421.
7 A. A. Popov, L. Zhang and L. Dunsch, *ACS Nano*, 2010, **4**, 795–802.
8 L. Dunsch and S. Yang, *Small*, 2007, **3**, 1298–1320.
9 S. Stevenson, G. Rice, T. Glass, K. Harich, F. Cromer, M. R. Jordan, J. Craft, E. Hadju, R. Bible, M. M. Olmstead, K. Maitra, A. J. Fisher, A. L. Balch and H. C. Dorn, *Nature*, 1999, **401**, 55–57.
10 M. Yamada, T. Akasaka and S. Nagase, *Acc. Chem. Res.*, 2010, **43**, 92–102.
11 N. B. Shustova, A. A. Popov, M. A. Mackey, C. E. Coumbe, J. P. Phillips, S. Stevenson, S. H. Strauss and O. V. Boltalina, *J. Am. Chem. Soc.*, 2007, **129**, 11676–11677.
12 N. B. Shustova, Y.-S. Chen, M. A. Mackey, C. E. Coumbe, J. P. Phillips, S. Stevenson, A. A. Popov, O. V. Boltalina and S. H. Strauss, *J. Am. Chem. Soc.*, 2009, **131**, 17630–17637.
13 L. Echegoyen, C. J. Chancellor, C. M. Cardona, B. Elliott, J. Rivera, M. M. Olmstead and A. L. Balch, *Chem. Commun.*, 2006, 2653–2655.
14 L. Zhang, A. A. Popov, S. Yang, S. Klod, P. Rapta and L. Dunsch, *Phys. Chem. Chem. Phys.*, 2010, **12**, 7840–7847.
15 A. A. Popov, S. Yang, M. Kalbac, P. Rapta and L. Dunsch, *AIP Conf. Proc.*, 2009, **1148**, 712–715.
16 A. A. Popov and L. Dunsch, *J. Am. Chem. Soc.*, 2008, **130**, 17726–17742.
17 P. Jakes and K. P. Dinse, *J. Am. Chem. Soc.*, 2001, **123**, 8854–8855.
18 T. Kato, *J. Mol. Struct.*, 2007, **838**, 84–88.
19 A. A. Popov and L. Dunsch, *J. Phys. Chem. Lett.*, 2011, **2**, 786–794.
20 B. Elliott, L. Yu and L. Echegoyen, *J. Am. Chem. Soc.*, 2005, **127**, 10885–10888.
21 A. A. Popov, N. B. Shustova, A. L. Svitova, M. A. Mackey, C. E. Coumbe, J. P. Phillips, S. Stevenson, S. H. Strauss, O. V. Boltalina and L. Dunsch, *Chem.–Eur. J.*, 2010, **16**, 4721–4724.
22 N. B. Shustova, D. V. Peryshkov, I. V. Kuvychko, Y.-S. Chen, M. A. Mackey, C. E. Coumbe, D. T. Heaps, B. S. Confait,

View Article Online

Published on 01 April 2011. Downloaded by Michigan State University on 22/01/2016 10:38:45.

T. Heine, J. P. Phillips, S. Stevenson, L. Dunsch, A. A. Popov, S. H. Strauss and O. V. Boltalina, *J. Am. Chem. Soc.*, 2011, **133**, 2672–2690.
23 T. Wang, J. Wu, W. Xu, J. Xiang, X. Lu, B. Li, L. Jiang, C. Shu and C. Wang, *Angew. Chem., Int. Ed.*, 2010, **49**, 1786–1789.
24 M. Munzarová, in *Calculation of NMR and EPR Parameters. Theory and Applications*, ed. M. Kaupp, M. Buhl and V. G. Malkin, Wiley-VCH Verlag GmbH & Co. KGaA, Weinheim, 2004, pp. 463–472.
25 M. L. Munzarová, P. Kubácek and M. Kaupp, *J. Am. Chem. Soc.*, 2000, **122**, 11900–11913.
26 T. Heine, K. Vietze and G. Seifert, *Magn. Reson. Chem.*, 2004, **42**, S199–S201.
27 A. A. Popov, C. Chen, S. Yang, F. Lipps and L. Dunsch, *ACS Nano*, 2010, **4**, 4857–4871.
28 A. Reich, M. Panthofer, H. Modrow, U. Wedig and M. Jansen, *J. Am. Chem. Soc.*, 2004, **126**, 14428–14434.
29 S. Taubert, M. Straka, T. O. Pennanen, D. Sundholm and J. Vaara, *Phys. Chem. Chem. Phys.*, 2008, **10**, 7158–7168.
30 W. Andreoni and A. Curioni, *Phys. Rev. Lett.*, 1996, **77**, 834–837.
31 J. M. Campanera, C. Bo, M. M. Olmstead, A. L. Balch and J. M. Poblet, *J. Phys. Chem. A*, 2002, **106**, 12356–12364.
32 R. Valencia, A. Rodriguez-Fortea, A. Clotet, C. de Graaf, M. N. Chaur, L. Echegoyen and J. M. Poblet, *Chem.–Eur. J.*, 2009, **15**, 10997–11009.
33 T. Wakahara, Y. Iiduka, O. Ikenaga, T. Nakahodo, A. Sakuraba, T. Tsuchiya, Y. Maeda, M. Kako, T. Akasaka, K. Yoza, E. Horn, N. Mizorogi and S. Nagase, *J. Am. Chem. Soc.*, 2006, **128**, 9919–9925.
34 C. Shu, C. Slebodnick, L. Xu, H. Champion, T. Fuhrer, T. Cai, J. E. Reid, W. Fu, K. Harich, H. C. Dorn and H. W. Gibson, *J. Am. Chem. Soc.*, 2008, **130**, 17755–17760.
35 K. Kobayashi and S. Nagase, *Chem. Phys. Lett.*, 1998, **282**, 325–329.
36 A. A. Goryunkov, I. V. Kuvychko, I. N. Ioffe, D. L. Dick, L. N. Sidorov, S. H. Strauss and O. V. Boltalina, *J. Fluorine Chem.*, 2003, **124**, 61–64.
37 E. I. Dorozhkin, D. V. Ignat'eva, N. B. Tamm, A. A. Goryunkov, P. A. Khavrel, I. N. Ioffe, A. A. Popov, I. V. Kuvychko, A. V. Streletskiy, V. Y. Markov, J. Spandl, S. H. Strauss and O. V. Boltalina, *Chem.–Eur. J.*, 2006, **12**, 3876–3889.
38 A. A. Popov, I. E. Kareev, N. B. Shustova, E. B. Stukalin, S. F. Lebedkin, K. Seppelt, S. H. Strauss, O. V. Boltalina and L. Dunsch, *J. Am. Chem. Soc.*, 2007, **129**, 11551–11568.
39 A. A. Popov, I. E. Kareev, N. B. Shustova, S. F. Lebedkin, S. H. Strauss, O. V. Boltalina and L. Dunsch, *Chem.–Eur. J.*, 2007, **14**, 107–121.
40 N. B. Shustova, I. V. Kuvychko, R. D. Bolskar, K. Seppelt, S. H. Strauss, A. A. Popov and O. V. Boltalina, *J. Am. Chem. Soc.*, 2006, **128**, 15793–15798.
41 I. E. Kareev, A. A. Popov, I. V. Kuvychko, N. B. Shustova, S. F. Lebedkin, V. P. Bubnov, O. P. Anderson, K. Seppelt, S. H. Strauss and O. V. Boltalina, *J. Am. Chem. Soc.*, 2008, **130**, 13471–13489.
42 F. Neese, *Inorg. Chim. Acta*, 2002, **337**, 181–192.
43 F. Neese, *J. Chem. Phys.*, 2001, **115**, 11080–11096.
44 F. Neese, *J. Chem. Phys.*, 2005, **122**, 034107.
45 J. P. Perdew, K. Burke and M. Ernzerhof, *Phys. Rev. Lett.*, 1996, **77**, 3865–3868.
46 D. N. Laikov, *Chem. Phys. Lett.*, 1997, **281**, 151–156.
47 D. N. Laikov and Y. A. Ustynuk, *Russ. Chem. Bull.*, 2005, **54**, 820–826.
48 A. A. Granovsky, *PC GAMESS/Firefly, version 7.1.C*, 2008, http://classic.chem.msu.su/gran/gamess/index.html.
49 F. Neese, *ORCA, an ab initio, density functional and semiempirical program package, version 2.7*, Institute for physical and theoretical chemistry, Bonn, 2009.
50 A. Schäfer, C. Huber and R. Ahlrichs, *J. Chem. Phys.*, 1994, **100**, 5829–5835.

 This journal is © the Owner Societies 2011